Enhanced luminescence at 2.88 and 2.04 μm from Ho3+/Yb3+ codoped low phonon energy TeO2–TiO2–La2O3 glass

GUPTA, Gaurav <http://orcid.org/0000-0002-2948-6740>, BALAJI, Sathravada <http://orcid.org/0000-0003-0820-6444>, BISWAS, Kaushik and ANNAPURNA, Kalyandurg

Published version

GUPTA, Gaurav, BALAJI, Sathravada, BISWAS, Kaushik and ANNAPURNA, Kalyandurg (2019). Enhanced luminescence at 2.88 and 2.04 μm from Ho3+/Yb3+ codoped low phonon energy TeO2–TiO2–La2O3 glass. AIP Advances, 9, 045201.

AIP Advances

Enhanced luminescence at 2.88 and 2.04 μm from Ho^{3+}/Yb^{3+} codoped low phonon energy TeO_2–TiO_2–La_2O_3 glass

Cite as: AIP Advances **9**, 045201 (2019); https://doi.org/10.1063/1.5054190
Submitted: 30 August 2018 . Accepted: 21 February 2019 . Published Online: 01 April 2019

Gaurav Gupta, Sathravada Balaji, Kaushik Biswas, and Kalyandurg Annapurna

Enhanced luminescence at 2.88 and 2.04 μm from Ho^{3+}/Yb^{3+} codoped low phonon energy TeO_2–TiO_2–La_2O_3 glass

Cite as: AIP Advances 9, 045201 (2019); doi: 10.1063/1.5054190
Submitted: 30 August 2018 • Accepted: 21 February 2019 •
Published Online: 1 April 2019

Gaurav Gupta, Sathravada Balaji, Kaushik Biswas, and Kalyandurg Annapurna[a)]

AFFILIATIONS

Glass Science and Technology Section, CSIR-Central Glass and Ceramic Research Institute, 196, Raja S. C. Mullick Road, Kolkata 700 032, India

[a)]Author to whom correspondence should be addressed; electronic mail: annapurnak@cgcri.res.in

ABSTRACT

The high phonon energy and short infrared cut-off wavelength of conventional oxide glass (or crystal) hosts are the limitations to achieve mid-infrared (MIR, λ≥2.5μm) luminescence. In present study, the luminescence performance of low phonon and non-conventional TeO_2-TiO_2-La_2O_3-based glass (TTL) host doped with Ho^{3+} and Ho^{3+}/Yb^{3+} has been investigated, for visible to MIR range. The MIR emission band with peak at 2.88μm (Ho^{3+}:$^5I_6 \rightarrow {}^5I_7$) and NIR band at 2.04μm (Ho^{3+}:$^5I_7 \rightarrow {}^5I_8$) has been realized from Ho^{3+} singly doped TTL glass due to low phonon energy and extended transmission window of the host. Intensity of MIR and NIR emission bands have enhanced significantly in Ho^{3+}/Yb^{3+}: TTL glass under Yb^{3+} excitation, signifying an efficient $Yb^{3+} \rightarrow Ho^{3+}$ energy transfer. The Judd-Ofelt analysis, on Ho^{3+} absorption characteristics reveals relatively better radiative transition probability ($34.4s^{-1}$) and branching ratio (10.5%), which is associated to Ho^{3+}:$^5I_6 \rightarrow {}^5I_7$ transition. The effective bandwidth of 2.88μm emission band is 180nm, with stimulated emission cross-section is $4.26\times10^{-21}cm^2$ and its gain bandwidth has been evaluated as $7.67\times10^{-26}cm^3$. For 2.04μm (Ho^{3+}:$^5I_7 \rightarrow {}^5I_8$) emission band, the effective bandwidth of 160.5nm and gain bandwidth of $7.26\times10^{-26}cm^3$ have been accomplished. The non-resonant Förster-Dexter method has been applied to Ho^{3+}/Yb^{3+}: TTL glass on emission (donor, Yb^{3+}) and absorption (acceptor, Ho^{3+}) cross sections. The evaluated donor-donor (C_{DD}) and donor-acceptor (C_{DA}) energy transfer micro-parameters are 1.02×10^{-38} and $5.88\times10^{-41}cm^6/s$ respectively while, maximum energy transfer efficiency has been 80%. In concise, Ho^{3+}/Yb^{3+} codoped TeO_2–TiO_2–La_2O_3 glass host has revealed its potential for MIR to NIR photonic applications.

I. INTRODUCTION

MIR lasers operating at 2–5μm are of huge significance as various gas-groups and hazardous chemicals are having their absorption bands around this wavelength range – thus making it useful in environmental pollution monitoring, chemical sensing, medical diagnostics, military countermeasures, and light detection and ranging (LIDAR) applications.[1–3] Currently, Optical Parametric Oscilloscope (OPO) and Quantum Cascade Lasers (QCL) are commercially available as MIR source.[4] However, the requirement of highly coherent monochromatic excitation source and significant dissipation of input power, have been the major limitations which, prevent their use in comparatively high power applications.[4] Therefore, cost-effective broadband MIR source with high output power is a challenge to accomplish. Single crystal, transparent ceramic or glass doped with suitable lanthanide ions operating at 2–5μm can be the plausible solution to realize efficient high power MIR source. Apart from MIR emission, efficient NIR luminescence for 1.55 – 2.0μm range has applications in eye-safe lasers, medical surgeries like laser scalpel and remote sensing etc.[5,6] The efficient NIR and MIR luminescence such as- Tm^{3+} at 1.9μm, Er^{3+} at 1.55 and 2.7μm, Ho^{3+} at 2.0 and 2.9μm, and Dy^{3+} at 2.9μm, are capable of. However, Ho^{3+} based lasers are of immense interest because 2.9 and 2.0μm emission bands are used extensively in medical surgery. Furthermore, the Ho^{3+} based laser has potential applications for optical detection, sensing of gas species and environmental quality control etc.[2] Reports are available which demonstrate the effectiveness of single crystal or transparent ceramic as solid state laser

material host that can be operated at MIR range.[7–10] However, the methods involved in synthesizing single crystal are expensive, time consuming and complicated.[11] While synthesis of transparent ceramics requires high temperature and pressure; furthermore, limitations of ceramics are- porous nature, segregation of dopant ions and limited compositions to use.[12] Hence, glasses doped with suitable lanthanide ion can be a reasonable solution to achieve cost effective, broadband and high power MIR lasers.[4] In this regard, most conventional SiO_2-based glass possesses robust structure, thermal stability, mechanical and chemical durability, but their maximum phonon energy is ~1100cm^{-1} and infrared cutoff wavelength being at 2.5μm, which limits their working wavelength range from visible to NIR (0.3μm–2.2μm).[13] Therefore, chalcogenide, fluoride and oxyfluoride systems have been investigated extensively due to their low phonon energy (350–630cm^{-1}) and high transparency in MIR range.[13] Chalcogenide hosts have exhibited transmission window from 0.45 to 11μm and low phonon energy (~350cm^{-1}). However, high linear refractive index (2.0–3.3), low glass transition temperature (300–420°C), poor thermal stability, chemical durability and less solubility to rare-earth ions have limited their use for photonic applications.[13] In case of fluoride and oxy-fluoride system MIR luminescence at 2.7μm owing to Er^{3+} ion and 2.9μm from Ho^{3+} ion has been reported.[15,16] Nevertheless, the synthesis of fluoride or oxy-fluoride glass under controlled atmosphere at high temperature (1400–1500°C) as well as the use and volatilization of corrosive element like fluorine is their major limitation for commercialization.[17] Recently Yoshimoto *et. al.*,[18] published the occurrence of Er^{3+}-based 2.7μm Mid-Infrared emission in $x$$Er_2O_3$–(50 – x) La_2O_3–50Ga_2O_3 glasses prepared via an aerodynamic levitation technique. However, the expensive and technological complexities are the major limitation for commercialization of these systems.

On the other hand, TeO_2-based glasses having suitable phonon energy (650–750cm^{-1}), extended transmission window (0.4–6μm), high solubility of rare-earth ions (~15mol%), considerable glass transition temperature (350–450°C), thermal stability (60–120°C), refractive index (n ~2.1), mechanical durability and zero dispersion wavelength (λ_{ZDW} ~2.3μm). Therefore, these glass hosts are most promising for MIR photonic applications.[14] Reports are available, demonstrating rare earth (RE^{3+}) activated MIR luminescence from TeO_2 based glasses.[13] In this regard, present efforts aimed at describing the effectiveness of Ho^{3+} ion doped and Ho^{3+}/Yb^{3+} co-doped TeO_2–TiO_2–La_2O_3 (TTL)-based oxide glass hosts, for broadband MIR and NIR photonic applications. The luminescence property of Ho^{3+} singly doped TTL glass, has been judged against Ho^{3+}/Yb^{3+} co-doping. The absorption spectra of Ho^{3+} ion singly doped in TTL glass are considered for theoretically evaluating the phenomenological Judd-Ofelt[19,20] parameters. The phenomenological parameters are used to predict the radiative transition probabilities, branching ratio and radiative lifetime corresponding to significant emission transition. Several fold enhancements in MIR (2.88μm) emission from Yb^{3+} sensitized, Ho^{3+} activated TTL glasses has been achieved, compare to Ho^{3+} singly doped glasses. Apart from MIR, intense and broad NIR luminescence at 2.04μm has been realized from Ho^{3+}/Yb^{3+}: TTL glass with FWHM of 160.5nm. The measured luminescence decay curves for Yb^{3+}:$^2F_{5/2}$ at 1006nm have been used to predict the energy transfer efficiency with energy transfer rates for Yb^{3+}→Ho^{3+}. Further the Inokuti-Hirayama and Brushtein models were applied to predict energy transfer mechanism for the present system. In precise, oxide-based TTL glass codoped with suitable RE^{3+} ions is a promising host to achieve broadband MIR and NIR luminescence with low threshold values for photonic applications.

II. EXPERIMENTAL PROCEDURES

Glasses with composition (in mol %) [80TeO_2- 10TiO_2-(10-x-y) La_2O_3- $x$$Ho_2O_3$- $y$$Yb_2O_3$] (i) Ho_2O_3 singly doped (designated as TTL-xHo) with y=0, x=0, 0.1, 0.3, 0.7, 1.0 mol% (ii) Ho^{3+}/Yb^{3+} codoped keeping y=1.0 constant (designated as TTL-Yb-xHo) with x=0, 0.1, 0.3, 0.7, 1.0 mol% were prepared by conventional melt quenching technique. Reagent grade chemicals such as TeO_2 (Alfa Aesar), TiO_2 (Sigma Aldrich) and La_2O_3, Ho_2O_3, Yb_2O_3 (Alfa Aesar) with purity ≥ 99.99% were used as raw materials for glass preparation. Batches weighing of 6g were mixed well and transferred in to platinum crucible at 900°C for 1h with intermittent stirring to achieve homogeneous and bubble-free melt followed by casting on preheated stainless steel mould. The glass samples were annealed at 350°C (near T_g) for 2h and slowly cooled down to room temperature to obtain thermal stress-free samples. The density of the glass samples was measured by using the Archimedes' buoyancy principle, using double distilled water as an immersion liquid on Mettler-Tollado digital mono-pan balance attached with density measurement kit. The refractive indices of all the samples were measured using Metricon M 2010 prism coupler (USA) equipped with five different wavelengths (473, 532, 632.8, 1064 and 1552 nm). To measure the IR transmission band edge and OH^- content in the prepared glasses, infrared transmission spectra were recorded, using FTIR spectrophotometers (spectral range 7800 to 400 cm^{-1}) (model: Frontier FIR MIR from Perkin-Elmer, UK). The UV-Vis-NIR optical absorption spectra were recorded in 200-2500 nm spectral range by using UV-Vis-NIR spectrophotometer (Model: 3101 from Shimadzu, Japan). The emission and excitation spectra of the sample were recorded at room temperature on spectrofluorimeter (Model: Quantum Master enhanced NIR from PTI, USA) fitted with double monochromators on both excitation and emission channels. The NIR (1500–2500 nm) and MIR (2500–4000 nm) emission spectra were recorded using different detectors with Xenon lamp operating as excitation source. For NIR and MIR region, instrument is equipped with solid state photodiode based InGaAs and LN_2 cooled InSb detectors respectively. The emission channels were equipped with 4000 nm blazed gratings for InSb detector. LN_2 cooled gated, near infrared (NIR) photo-multiplier tube (Model: NIR-PMT-R 1.7, Hamamatsu) was used to acquire Vis-NIR emission as well as fluorescence decay, using Xenon lamps of 60 W powers as source. All the measurements were carried out by placing the sample at 60° to the incident beam and signals were collected from same surface at right angle (90°) to the incident beam. Appropriate low-pass and high-pass filters from Edmund Optics, Inc, USA were used at excitation and emission channels to avoid excitation and emission wavelength's higher order harmonics in the recorded emission spectrum.

III. RESULTS AND DISCUSSIONS

A. Optical absorption spectra

The detailed analysis of physical, mechanical, thermal and optical properties of base glass [in mol% 80TeO_2–10TiO_2–10La_2O_3]

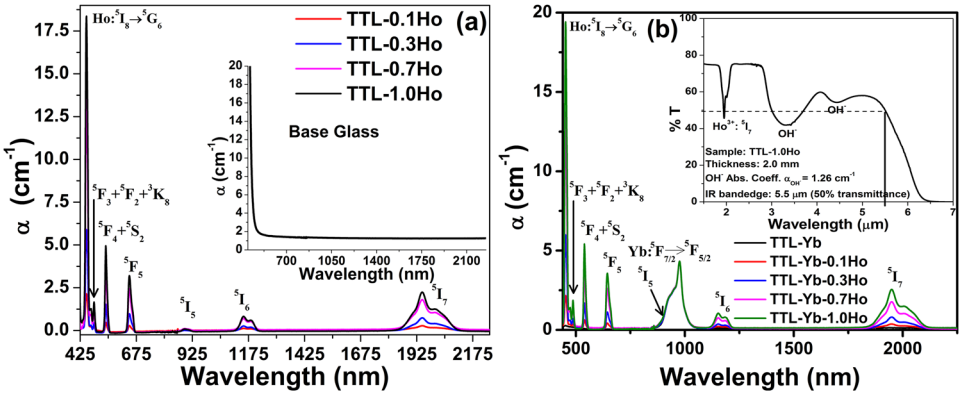

FIG. 1. Baseline corrected absorption coefficient for (a) Ho^{3+} doped glasses (inset: base glass) and (b) Yb^{3+} and Ho^{3+}/Yb^{3+} codoped glasses (inset: FTIR transmission spectra for MIR to FIR range).

(TTL) has been reported previously.[14] Through the present study, the spectroscopic properties of Ho^{3+} doped and Ho^{3+}/Yb^{3+} codoped TeO_2–TiO_2–La_2O_3 (TTL) glass host have been explored. Absorption coefficient (α) of TTL: Ho^{3+} singly doped and TTL: Ho^{3+}/Yb^{3+} codoped glasses are presented in Fig. 1(a) and (b) respectively. An inset of Fig. 1(a) is representing the absorption coefficient of base glass. Inset of Fig. 1(b) describes the extended transmission spectra of TTL-1.0Ho glass, which reveals the presence of OH^- ion impurity with absorption coefficient α_{OH^-}=1.26 cm^{-1}. IR edge for 50% transmittance is realized at 5.5 μm, signifying the capability of MIR luminescence from TTL glass. In the previous investigation authors have reported that the material zero dispersion wavelength (λ_{ZDW}) is at 2.28 μm for undoped TTL (or, TTL10) glass, suggesting that the present glass host can be operated from visible (λ> 0.4μm) to MIR (λ< 3.5 μm) regions for photonic applications.[14]

B. Judd-Ofelt analysis

The baseline corrected absorption spectra have been used to perform Judd-Ofelt (J-O) analysis following standard procedures.[19–21] The Reduced matrix elements were adopted from Kaminskii to perform J-O analysis.[22] The Ho^{3+} ion concentration dependent line strengths were measured experimentally as well as theoretically (not shown in the Table) with calculated phenomenological J-O parameters (Ω_λ, λ= 2, 4, 6), sum of phenomenological parameters ($\Sigma_\lambda\Omega_\lambda$), root mean square deviation in line strength (ΔS_{rms}) and the degree of covalency (η) has been presented in Table I.

TABLE I. The Ho^{3+} ion concentration (N_{Ho}), phenomenological J-O parameters (Ω_λ, λ=2, 4, 6), sum of phenomenological parameters ($\Sigma_\lambda\Omega_\lambda$), root mean square deviation in line strength (ΔS_{rms}) and degree of covalency (η).

Properties	TTL-0.3Ho	TTL-0.7Ho	TTL-1.0Ho
N_{Ho} ($\times10^{20}$ cm^{-3})	1.21	2.79	4.00
Ω_2 ($\times10^{-20}$ cm^2)	5.06	4.80	4.39
Ω_4 ($\times10^{-20}$ cm^2)	3.90	3.88	3.52
Ω_6 ($\times10^{-20}$ cm^2)	1.04	1.08	0.98
$\Sigma_\lambda\ \Omega_\lambda$ ($\times10^{-20}$ cm^2)	10.0	9.76	8.90
ΔS_{rms} ($\times10^{-20}$ cm^2)	0.19	0.21	0.23
η	0.602	0.589	0.582

Considerably small values of root mean square deviation (ΔS_{rms}) imply the reliability of the calculated J-O parameters. According to Table I, phenomenological Ω_2 and Ω_4 parameters decrease steadily with increase of Ho^{3+} ion concentration, whereas Ω_6 remains approximately unaltered and, moreover, $\Omega_2>\Omega_4>\Omega_6$ for the present series of glasses. According to Kumar *et. al.*, phenomenological parameters Ω_2 and Ω_4 are strongly associated to the hypersensitive transitions.[23] The phenomenological parameters can be expressed as,[24]

$$\Omega_t = (2t+1)\sum_{p,s}|A_{sp}|^2\Xi^2(s,t)(2s+1)^{-1} \quad (1)$$

where A_{sp} are the crystal field parameters of rank "S", which are related to the structure around the RE^{3+} ion; the parameter $\Xi(s,t)$ is related to the matrix elements between two radial wave-functions of *4f* and admixing levels like *5d* and *5g* and the energy difference between these two levels.[23] The parameter $\Xi(s,t)$ is directly proportional to the degree of covalency (η) of the RE^{3+}–O^{2-} bond.[23] In the present study glass composition remains more or less unaltered with the only increase of Ho_2O_3 content in the network by progressive substitution of La_2O_3; thus the crystal field parameters are unaltered. Therefore, the degree of covalency is exclusively affecting J-O parameters. Thus to quantify the degree of covalency (η), Kumar *et. al.*, devised a formula that can be written as,[23]

$$\eta = I_L/I_S \quad (2)$$

where I_L and I_S are the intensities of Stark component for long and short wavelengths transition respectively, corresponding to hypersensitive band. The decrease in "η" implies the decrease in the covalency of the rare earth-ligand (RE^{3+}–O^{2-}) bond. In case of Ho^{3+} ion, the hypersensitive transition is $^5I_8\rightarrow{}^5G_6$, thus intensity ratio of its Stark components is useful to quantify "η". The degree of covanlency has been estimated for the studied Ho^{3+}: TTL glasses and the data are presented in Table I. It is clearly observed that, the increase of Ho^{3+} ion concentration leads to steady decrease in Ω_2 and Ω_4 parameters for present series of glasses, which can be attributed to the steady decrease in degree of covalency (η). Further, according to Oomen and Van Dongen, it is convenient to look at the sum of J-O parameters ($\Sigma_\lambda\ \Omega_\lambda$), that decreases consistently with covalency, rather than single Ω_λ parameter.[25] In the present case also, the prominent decrease of $\Sigma_\lambda\ \Omega_\lambda$ with increase in dopant ion

TABLE II. Comparative study of J-O parameters (Ω_λ, λ= 2, 4, 6) (in 10^{-20}cm^2) for Ho^{3+} ions doped in different glass hosts.

Host glass composition	Ω_2	Ω_4	Ω_6
ZrF_4–BaF_2–$A1F_3$–NaF–LaF_3 (ZBLAN)[26]	2.43	1.67	1.84
SiO_2–Al_2O_3–Na_2O–ZnF_2[27]	5.84	2.38	1.75
ZnO–Al_2O_3–Bi_2O_3–B_2O_3[28]	13.01	3.63	0.41
PbO–PbF_2[29]	5.60	2.72	1.87
TeO_2–TiO_2–La_2O_3 [Present]	5.08	3.90	1.04

concentration is in agreement with the decrease of the degree of covalency (η) as presented in Table I. The calculated Ω_λ parameters for present TTL host have been compared with fluoride, oxyfluoride, zinc-boro-bismuthate, lead-oxyfluoride glass host doped with Ho^{3+} ion and presented in Table II.[26–29] As described in Table II, the higher values of Ω_2 parameter compared to present host has been noticed in bismuth or lead-based oxide or oxyfluoride glasses, whereas in the case of fluoride lower value is depicted. In this context, Jorgensen *et al.* and Ebendorff-Heidepriem *et. al.*, described the strong dependency of Ω_2 parameter on asymmetry of ligand, in addition to the covalency of RE^{3+} ion site.[24,30] The presence of a heavy metal (Bi or Pb) in the glass network or in case of oxyfluoride system the asymmetry in the ligand field causes the enhancement in Ω_2 parameter. Fluoride glass is showing significantly small Ω_2 due to the smaller electric field gradient of monovalent fluoride compared to divalent oxide ion. Hence, due to presence of Te in the network of the present TTL glasses, Ω_2 parameter in this case is lower than those of bismathate/lead/oxyfluoride glasses and higher than those regarding fluoride glasses. The phenomenological Ω_4 parameter depends on the optical basicity of the network; Table II suggests that present TTL host has considerable optical basicity. According to Tanabe *et al.*, in comparison with Ω_2, phenomenological parameter Ω_6 depends less on the local environment of RE^{3+} ion, though it is strongly correlated with the rigidity of the glass network with overlapping of *4f* and *5d* orbitals.[31] According to the present study, TTL glass is exhibiting smaller value of Ω_6 compared to other glass systems as reported in Table II except ZnO–B_2O_3–Bi_2O_3–Al_2O_3 system. It is suggesting that the electron density of Ho^{3+} ion in *6s* orbital is smaller with less network rigidity in the present host, which can be attributed to the presence of low electronegative modifier such as Ti^{4+} and La^{3+} ion in the network. On the basis of computed phenomenological J-O parameters, radiative properties such as radiative transition probability (A_{rad}), branching ratio (β) and total radiative lifetime (τ_{rad}) have been estimated and presented in Table III. The radiative transition probability for $^5(S_2, F_4)\rightarrow{}^5I_8$ transition is 2215s^{-1} which is responsible for intense green emission at 0.55μm; while transitions related to NIR/MIR emissions are found to be 132.4 s^{-1} ($^5I_7\rightarrow{}^5I_8$, λ_{em}: 2.04 μm) and 34.4 s^{-1} ($^5I_6\rightarrow{}^5I_7$, λ_{em}: 2.88 μm), which appear to be higher compared to fluoroaluminate glass and fluoride.[32,33] Enhanced radiative lifetime with suitable branching ratio is essential to achieve intense fluorescence, which can contribute to efficient MIR or NIR lasing. In the following section, the experimentally realized emission spectra extended from visible to MIR range has been presented under various excitations wavelengths.

TABLE III. Calculated values of radiative transition probabilities (A_{rad}), branching ratio (β) from J-O parameter and calculated total radiative lifetime (τ_{rad}).

		TTL-0.3Ho		TTL-0.7Ho		TTL-1.0Ho	
Emission Transition	Energy (cm^{-1})	A_{rad} (s^{-1})	β (%)	A_{rad} (s^{-1})	β (%)	A_{rad} (s^{-1})	β (%)
$^5I_7\rightarrow{}^5I_8$	5150	129.0	100	132.0	100	120.0	100
τ_{rad} (ms)		7.72		7.55		8.33	
$^5I_6\rightarrow{}^5I_7$	3500	34.0	10.6	34.4	10.5	31.1	10.5
$^5I_8$	8540	286	89.4	294	89.5	266.0	89.5
τ_{rad} (ms)		3.13		3.05		3.36	
$^5F_5\rightarrow{}^5I_4$	2300	0.2	0.00	0.2	0.00	0.2	0.00
$^5I_5$	4350	15	0.2	15	0.2	14	0.2
$^5I_6$	6910	203	3.0	205	3.0	186	3.0
$^5I_7$	10410	1253	18.2	1255	18.2	1140	18.2
$^5I_8$	15450	5415	78.6	5439	78.7	4942	78.7
τ_{rad} (ms)		0.15		0.14		0.16	
$^5(S_2, F_4)\rightarrow{}^5F_5$	2740	1.2	0.0	1.2	0.0	1.0	0.0
$^5I_4$	5030	65	1.7	66	1.7	60	1.7
$^5I_5$	7090	59	1.5	61	1.5	55	1.5
$^5I_6$	9650	287	7.4	294	7.3	266	7.3
$^5I_7$	13150	1334	34.4	1386	34.5	1258	34.5
$^5I_8$	18190	2133	55.0	2215	55.1	2010	55.1
τ_{rad} (ms)		0.26		0.25		0.27	

C. Emission and excitation spectra

1. Ho^{3+} doped TTL glasses

The recorded Ho^{3+} ion concentration dependent luminescence spectra extended from visible (0.5μm) to MIR (3.5μm) has been depicted in Fig. 2(a) and (b). The partial energy level diagrams of Ho^{3+} ion with possible excitation and emission transitions are illustrated in Fig. 2(c). The insets of Fig. 2(a) and (b) has been depicting the excitation spectra corresponding to major emission transitions. Figure 2(a) reveals emission spectra extended from visible to NIR (0.5– 1.5μm) which demonstrate strong green (λ_{em}: 0.549μm; Ho^{3+}:$^5(S_2, F_4)\rightarrow{}^5I_8$), weak red ($\lambda_{em}$: 0.659μm; Ho^{3+}:$^5F_5\rightarrow{}^5I_8$) emission following NIR luminescence bands like (λ_{em}: 0.757μm; Ho^{3+}:$^5(S_2, F_4)\rightarrow{}^5I_7$), ($\lambda_{em}$: 0.981μm; Ho^{3+}:$^5F_5\rightarrow{}^5I_7$), (λ_{em}: 1.02μm; Ho^{3+}:$^5(S_2, F_4)\rightarrow{}^5I_6$), ($\lambda_{em}$: 1.194μm; Ho^{3+}:$^5I_6\rightarrow{}^5I_8$) and (λ_{em}: 1.38μm; Ho^{3+}:$^5(S_2, F_4)\rightarrow{}^5I_5$) respectively under blue excitation (λ_{ex}: 0.453μm; Ho^{3+}:$^5I_8\rightarrow{}^5G_6$). The inset of Fig. 2(a) is presenting the excitation spectra corresponding to λ_{em}: 0.55μm evidently demonstrating intense excitation band at 0.453μm. The NIR and MIR emission bands at λ_{em}: 2.04μm and λ_{em}: 2.88μm owing to inter-manifold transition Ho^{3+}:$^5I_7\rightarrow{}^5I_8$ and Ho^{3+}:$^5I_6\rightarrow{}^5I_7$ under excitation at λ_{ex}: 1.194μm has been presented in Fig. 2(b). Inset of Fig. 2(b) have been depicting the excitation spectra of 2.04 and 2.88μm emission bands. Excitation spectra reveal the most efficient wavelength is at 1.194μm. It is interesting to observe that, luminescence bands originating from $^5(S_2, F_4)$ and $^5I_6$ levels such as $^5(S_2, F_4)\rightarrow{}^5I_{7,6,5}$, $^5F_5\rightarrow{}^5I_7$ and $^5I_6\rightarrow{}^5I_7$ has been realized for Ho^{3+}: TTL glass, which can be resulted in the low phonon energy of the system. For Ho^{3+} singly doped TTL glasses, two emission bands at visible wavelength have been realized. The peak wavelength of the emission bands are realized at 549 nm (Ho^{3+}: $^5(S_2, F_4)\rightarrow{}^5I_8$), 659 nm ($Ho^{3+}$: $^5F_5\rightarrow{}^5I_8$) and 549 nm (Ho^{3+}: $^5(S_2, F_4)\rightarrow{}^5I_7$) respectively. The radiative transition probability associated with these emission bands can be written as,

$$A_{rad}(549nm) = \frac{64n\left(n^2+2\right)^2\pi^4e^2}{27h\lambda_p{}^3g_j}\left(0\times\Omega_2+0\times\Omega_4+0.227\times\Omega_6\right) \quad (3a)$$

$$A_{rad}(659nm) = \frac{64n\left(n^2+2\right)^2\pi^4e^2}{27h\lambda_p{}^3g_j} \times\left(0\times\Omega_2+0.4278\times\Omega_4+0.5686\times\Omega_6\right) \quad (3b)$$

$$A_{rad}(757nm) = \frac{64n\left(n^2+2\right)^2\pi^4e^2}{27h\lambda_p{}^3g_j}\left(0\times\Omega_2+0\times\Omega_4+0.4097\times\Omega_6\right) \quad (3c)$$

For the above equations n is the refractive index of the host at emission peak wavelength (λ_p), g_j is the multiplicity of the excited state involved in the emission transition, e is the electric charge of electron and h is the Planck's constant. However, the initial multiplication factors remain constant for various concentrations of Ho^{3+} ion. The constant multiplication factors in the parenthesis are corresponds to the reduced squared matrix, these are multiplied with the Judd-Ofelt parameters (Ω_λ). Therefore, radiative transition probability associated with certain emission transition at various concentrations of Ho^{3+} ion, is dependent on the terms involved in the parenthesis.

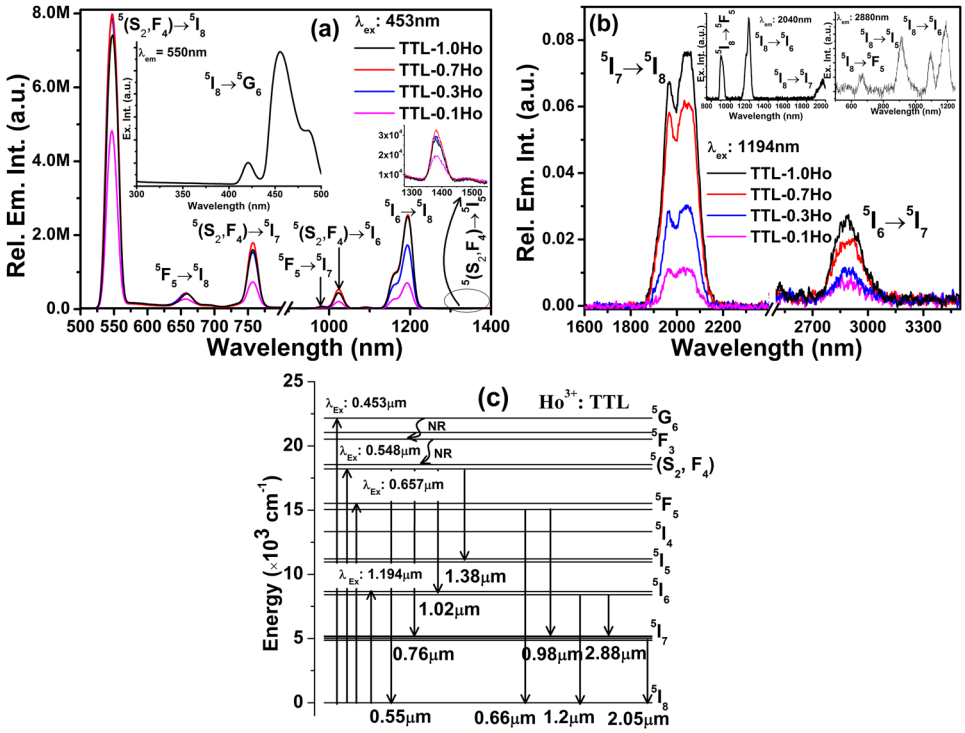

FIG. 2. Emission spectra for concentration dependent Ho^{3+} singly doped TTL glasses extended from (a) visible (0.5μm) to NIR (1.5μm) range under 0.453μm excitation (inset: excitation spectra for 0.55μm emission peak) and (b) NIR (1.6μm) to MIR (3.5μm) using excitation at 1.194μm (inset: excitation spectra for 2.05 and 2.88μm emission peak), (c) partial energy level diagram for TTL: Ho^{3+} with excitation and emission transitions.

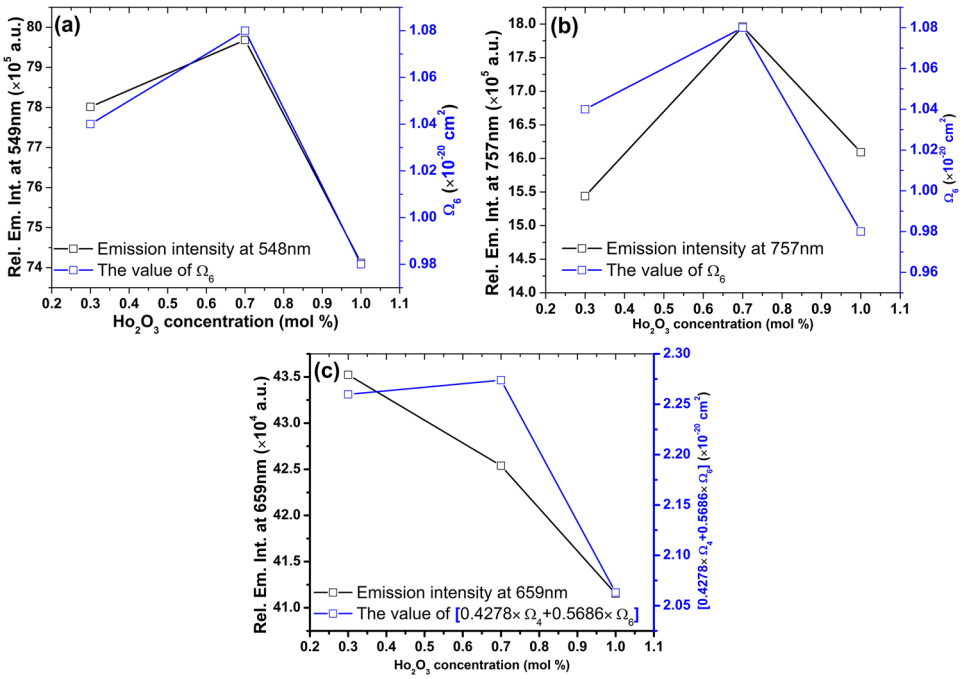

FIG. 3. The variation of measured visible emission peak intensity at (a) 549 nm, (b) 757 nm and (c) 659 nm along with collective effects of J-O parameters, for various concentrations of Ho_2O_3 in TTL host.

Hence, it is evident that the radiative transition probability associated with Ho^{3+}: $^5(S_2, F_4) \rightarrow {}^5I_8$ transition is independent of Ω_2 and Ω_4, but depends on the Ω_6. The relative emission intensity at 549nm and numerical value of Ω_6 parameter has been plotted against Ho_2O_3 concentration in the TTL network which has been presented as Fig. 3(a). Analogous approach has been adopted for the 757 nm emission band. The relative emission intensity at 757 nm for various concentrations of Ho_2O_3 has been plotted with Ω_6 parameter and the respective trend has been depicted in the Fig. 3(b). In case of 659 nm emission band, the radiative transition probability involves both Ω_4 and Ω_6. Therefore, the trend of emission intensity at 659nm has been plotted with $(0.4278\times\Omega_4 + 0.5686\times\Omega_6)$ factor, which has been exhibited in the Fig. 3(c). Fig. 3(a) and (b), reveal that the emission intensity of 549 and 757 nm has been following the same trend as Ω_6 parameter. On the contrary, the emission intensity at 659nm has been following the trend of $(0.4278\times\Omega_4 + 0.5686\times\Omega_6)$ factor. The trends of measured emission intensities have been following precisely with theoretical J-O parameter; thus experimentally validating the theoretical predictions of radiative transition probability. Moreover, this establishes the dependence of Ω_λ parameter with the emission intensity.

From Fig. 2(a), the experimental branching ratio corresponding to recorded emission transitions from $^5(S_2, F_4)$ manifold to its subsequent lower energy levels has been evaluated through the ratio of area under the respective curves to that of total area (β_{exp}) and compared with theoretically evaluated values ($\beta_{J\text{-}O}$) presented in Table IV. According to Table IV, the experimental branching for the transition $^5(S_2, F_4) \rightarrow {}^5I_8$ is higher than that of predicted value and as a consequence, branching ratio for transitions to other lower energy levels is lower than its $\beta_{J\text{-}O}$. Further it can be seen that with the increase of Ho^{3+} concentration in the network, experimental branching ratio corresponding to $^5(S_2, F_4) \rightarrow {}^5I_8$ transition decreases steadily with the simultaneous increase in $^5(S_2, F_4) \rightarrow {}^5I_{7,6}$ transitions, this can be attributed to the enhanced ion-ion energy transfer at higher Ho^{3+} concentration. The TTL-0.7Ho sample demonstrates the maximum luminescence intensity under 0.453μm

TABLE IV. Comparison between experimentally measured (β_{exp}) and theoretically calculated ($\beta_{J\text{-}O}$) branching ratio for the emission transitions related to $^5(S_2, F_4)$ manifold.

Sample→	TTL-0.1Ho		TTL-0.3Ho		TTL-0.7Ho		TTL-1.0Ho	
Transition	β_{exp}	$\beta_{J\text{-}O}$	β_{exp}	$\beta_{J\text{-}O}$	β_{exp}	$\beta_{J\text{-}O}$	β_{exp}	$\beta_{J\text{-}O}$
$^5(S_2, F_4) \rightarrow {}^5I_8$	81.6	- -	79.4	55.0	77.2	55.1	77.7	55.1
$^5I_7$	13.4	- -	14.8	34.4	16.2	34.5	16.2	34.5
$^5I_6$	4.5	- -	5.3	7.4	6.1	7.3	5.5	7.3
$^5I_5$	0.5	- -	0.5	1.5	0.5	1.5	0.5	1.5

excitation. Under 1.194μm pumping, the maximum emission intensity at 2.04 and 2.88μm transition has been realized for TTL-1.0Ho sample. However, intensity of MIR (λ_{em}: 2.88μm) as well as NIR (λ_{em}: 2.04μm) emission bands are considerably weak in Ho^{3+} singly doped TTL glasses. The basis of this weak emission performance can be attributed to the weak absorption cross-section at around 1.19μm (pump wavelength) due to $^5I_8 \rightarrow {}^5I_6$ transition ($\sigma_{abs}{}^p = 3.5\times10^{-21}cm^2$) of Ho^{3+} ion. Furthermore, the unavailability of suitable excitation laser (λ: 1.19μm) sources with sufficient pump power is the major limitation to achieve intense MIR luminescence from Ho^{3+}singly doped systems. As described in Fig. 1(b), the peak absorption cross-section at λ_p: 0.978μm for Yb^{3+}:$^2F_{7/2} \rightarrow {}^2F_{5/2}$ transition has been found to be $\sigma_{abs}{}^p = 2.4\times10^{-20}cm^2$ which is signifying its potential as a sensitizer. For the enhancement of MIR and NIR luminescence from Ho^{3+} ion, the TTL glass has been codoped by Ho^{3+}/Yb^{3+} where Yb^{3+} ion is acting as sensitizer.

2. Ho^{3+}/Yb^{3+} codoped TTL glasses

The MIR and NIR related spectroscopic properties of Ho^{3+}/Yb^{3+} codoped TTL glass has been explored with varied Ho^{3+} ion concentration, while Yb_2O_3 concentration is kept constant at 1mol%. The activator (Ho^{3+}) ion concentration dependent, Yb^{3+} sensitized (λ_{ex}: 0.986μm), extended NIR (1.0–1.5μm), (1.6–2.5μm) and MIR (2.5–3.5μm) emission spectra has been depicted in Fig. 4(a), (b) and (c) respectively. Inset of Fig. 4(a) describes the excitation spectra for Yb^{3+}emission at 1.01μm. Insets of Fig. 4(b) have been depicting excitation spectra corresponding to Ho^{3+} emission at 2.04 μm. The emission cross-section for 2.88μm band using Fuchtbauer-Ladenberg equation, as well as excitation spectrum for emission at 2.88μm in Ho^{3+}/Yb^{3+} codoped TTL glass, has been illustrated in the inset of Fig. 4(c). The NIR emission spectra presented in Fig. 4(a) reveal emission bands at 1.01μm (Yb^{3+}: $^2F_{5/2} \rightarrow {}^2F_{7/2}$) and 1.194μm ($Ho^{3+}$: $^5I_6 \rightarrow {}^5I_8$) for Yb^{3+} singly doped as well as Ho^{3+}/Yb^{3+} codoped TTL glasses under 0.987μm excitation. With increase in Ho^{3+} ion concentration, emission band intensity at 1.01μm decreases steadily, implying the efficient $Yb^{3+} \rightarrow Ho^{3+}$ energy transfer. However, the 1.194μm emission band has been demonstrating maximum luminescence intensity for TTL-Yb-0.7Ho glass, entailing that for excitation at 0.987μm, concentration quenching is affecting luminescence intensity beyond 0.7mol% of Ho_2O_3 concentration in Ho^{3+}/Yb^{3+} codoped TTL glasses. As depicted in Fig. 4(b) and (c), about 10 fold enhancement in luminescence peak intensity at 2.04μm, and 6 fold enhancement in the MIR luminescence peak intensity at 2.88μm, for Ho^{3+}/Yb^{3+} codoped system under 0.986μm excitation, have been realized – compared to Ho^{3+} singly doped TTL glass excited at 1.194μm. However, the optimized luminescence intensity at 2.04 and 2.88μm has been realized for TTL-Yb-0.7Ho sample under 0.986μm excitation, which is the obvious consequence of concentration quenching at Ho^{3+}: $^5I_6$ manifold as realized in 1.194μm emission intensity. To estimate emission cross-section (σ_{em}) spectra corresponding to 2.88 and 2.04μm emission bands, the Fuchtbauer-Ladenberg (F-L) equation[33] has been adopted, and the equation can be described as,

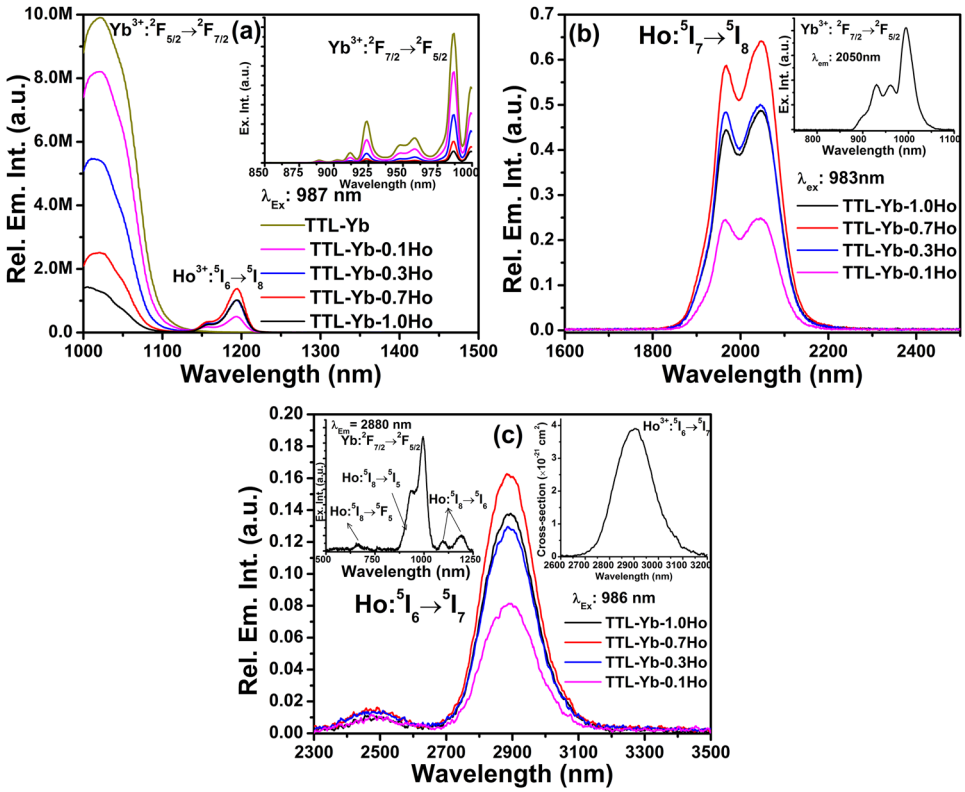

FIG. 4. Emission spectra for concentration dependent Ho^{3+}/Yb^{3+} codoped TTL glasses extended in (a) NIR (1.0–1.6μm) range (inset: excitation spectra for λ_{em}: 1.01μm), (b) NIR (1.6– 2.5μm) range (inset: excitation spectra for λ_{em}: 2.04μm), (c) MIR (2.5– 3.5μm) range (inset: excitation spectra for λ_{em}: 2.88μm and emission cross-section spectra corresponding to 2.88μm band).

$$\sigma_{em}(\lambda) = \frac{A_{rad}\lambda^4}{8\pi n^2 c} \times \frac{\lambda I(\lambda)}{\int \lambda I(\lambda) d\lambda} \quad (4)$$

Where A_{rad} is radiative transition probability; λ is wavelength; $I(\lambda)$ is the wavelength dependent emission intensity; c is the velocity of light in free space, and n is the refractive index of respective host. Inset of Fig. 4(c) depicts the emission cross-section for the MIR emission band. The bandwidth has been estimated as $\Delta\lambda$= 180nm related to emission band at 2.88μm which is comparable to our previously reported (TeO_2–BaO–BaF_2–La_2O_3) oxyfluoride system[34] but larger than chalcogenide (43nm),[35] fluoroaluminate (59nm),[33] TeO_2–Nb_2O_5–YF_3–GeO_2 glass (132nm)[36] and $LuLiF_4$ crystal (~50nm).[33] Further, the emission bandwidth realized for 2.04μm emission band is $\Delta\lambda$= 160.5nm. The enhanced MIR and NIR emission bandwidth of present host, is being attributed to the presence of various structural units like [TeO_4], [TeO_3] and [TeO_{3+1}].[14] Moreover, the composition partitioning in nano-scale, due to liquid-liquid immiscibility of present (i.e. TTL 10) host; has been responsible for enhanced emission bandwidth.[14] Important property of laser gain cross section associated with present host, has been discussed in the following section.

3. Gain cross section

In previous study, authors have elucidated the activator (Ho^{3+}) ion concentration dependent upconversion mechanism, of Ho^{3+}/Yb^{3+} codoped TTL glass under continuous (LD, λ_{ex}: 0.976μm) and pulsed excitations (unpublished data). However, the scope of discussion of frequency upconversion of present host will not encompass in present investigation. Therefore, on the basis of that frequency upconversion mechanism, under Yb^{3+} sensitization, the energy level diagram for Ho^{3+}/Yb^{3+} codoped system has been presented to Fig. 5(a). The gain curves for important emission bands at MIR (2.88μm) and NIR (2.04μm) are presented in Fig. 5(b) and (c) respectively. Insets of Fig. 5(b) and (c) are depicting the related absorption and emission cross sections. Using absorption and emission cross sections, the gain curves has been estimated; with the help of the formula given below,

$$\sigma_G(\lambda) = P \times \sigma_{em}(\lambda) - (1 - P) \times \sigma_{abs}(\lambda) \quad (5)$$

where $\sigma_G(\lambda)$ represents the gain cross section; P represents relative population density of ions in the related manifolds; thus ($0< P <1$), $\sigma_{em}(\lambda)$ and $\sigma_{abs}(\lambda)$ are presenting absorption and emission cross sections. However, the Ho^{3+}: $^5I_6 \rightarrow {}^5I_7$ transition responsible for 2.88μm emission band is an inter-manifold transition; therefore, respective absorption cross section has been considered on the basis of reciprocity theory as proposed by Zhou *et. al.*,.[33] The gain cross sections for MIR and NIR bands reveal that $P \geq 0.4$ is the population concentration, for which gain is positive – implying that attainment of laser threshold is possible at lower pump power. Hence, sufficiently intense MIR luminescence with suitable gain cross section has been realized for the Ho^{3+}/Yb^{3+}: TTL glass with small laser threshold. In the following section the energy transfer parameters for Ho^{3+}/Yb^{3+}: TTL glass has been evaluated using Förster-Dexter energy transfer method.

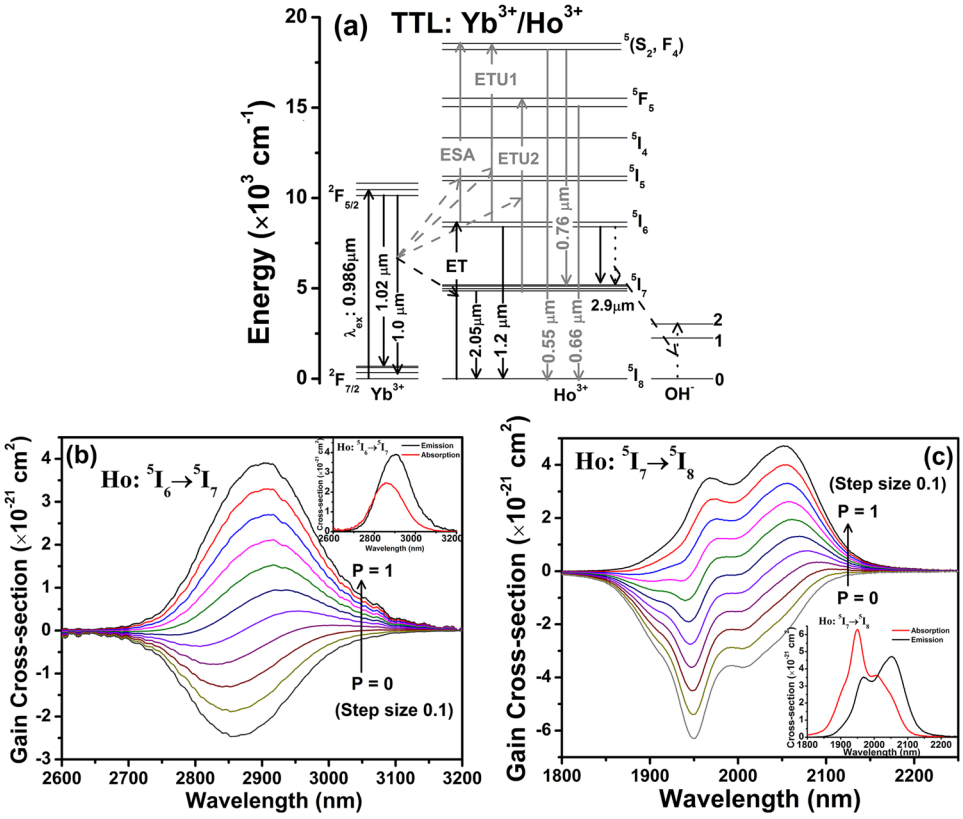

FIG. 5. (a) Partial energy level diagram for TTL: Ho^{3+}/Yb^{3+} under Yb^{3+} sensitization; gain cross section for (b) Ho^{3+}: $^5I_6 \rightarrow {}^5I_7$ (Inset: absorption and emission cross section for Ho^{3+}: $^5I_6 \rightarrow {}^5I_7$ transition) and (c) Ho^{3+}:$^5I_7 \rightarrow {}^5I_8$ (Inset: absorption and emission cross section for Ho^{3+}: $^5I_7 \rightarrow {}^5I_8$ transition) transitions.

D. Förster-Dexter energy transfer

The energy level diagram for Ho^{3+}/Yb^{3+} codoped system has been presented by Fig. 6(a). Exhibiting the $Yb^{3+} \rightarrow Ho^{3+}$ energy transfer is of non-resonant kind, while sensitized via Yb^{3+} ion. The Förster-Dexter proposed an equation to quantify the energy transfer micro-parameters (C_{DX}) where X can be donor (D) or acceptor (A) that can be expressed as:[37,38]

$$C_{DX} = \frac{3c}{8\pi^4 n^2} \int \sigma_{em}^{D}(\lambda)\sigma_{abs}^{X}(\lambda)d\lambda \quad (6)$$

where c represents the velocity of light in free space; refractive index of the medium is n; and $\sigma_{em}{}^{D}(\lambda)$ and $\sigma_{abs}{}^{X}(\lambda)$ are the emission and absorption cross sections of the donor and acceptor/donor, respectively. The emission cross section used in the equation (5) has been estimated using McCumber theory[39] which can be expressed as:

$$\sigma_{em}(\lambda) = \sigma_{abs}(\lambda)(Z_l/Z_u)\exp[(E_{ZL} - h\nu)/k_B T] \quad (7)$$

where Z_l and Z_u are presenting the degeneracy of the lower and upper manifolds involved in the transition respectively, while E_{ZL} is representing the zero level energy. However, because of non-resonant behavior of energy transfer, the Förster-Dexter equation cannot be directly applied to quantify respective energy transfer micro-parameters. Therefore, on the calculation of energy transfer micro-parameters by using the equation (5), the contribution due to phonon side bands should be considered. Hence contribution from Stokes phonon side bands in absorption and emission cross-section spectra has been estimated, using the exponential law proposed by Auzel[40] as given below,

$$\sigma_{Stokes} = \sigma_{elec}\exp(-\alpha_S \Delta E) \quad (8)$$

where the energy mismatch between electronic and vibronic transitions is ΔE and α_S is the host dependent parameter for Stokes transitions represented as,[41]

$$\alpha_S = (h\nu_{\max})^{-1}[\ln\{(N/S_0) \times (1 - \exp(-h\nu_{\max}/k_B T))\} - 1] \quad (9)$$

where number of phonons required for bridging the energy gap is N; the electron–phonon coupling constant is ($S_0 \approx 0.04$); $h\nu_{\max}$ is the maximum phonon energy of the host in present case ($h\nu_{\max} = 750 cm^{-1}$); k_B is the Boltzmann constant, and T stands for temperature, at room temperature ($k_B T \approx 208 cm^{-1}$). In the present case, TTL host ($\alpha_S = 3.85\times10^{-3} cm$) has been applied to estimate the cross section in the phonon side bands as presented in Fig. 6(a). The modified absorption and emission cross section has been adopted in the equation (5) to estimate the donor–donor and donor-acceptor energy migration micro-parameter terms defined as C_{DD} and C_{DA} respectively. As described in Figure 5(a), the estimated C_{DD} and C_{DA} are 1.02×10^{-38} and $5.88\times10^{-41} cm^6/s$ respectively, suggesting that compared to donor-acceptor, the donor-donor energy transfer is more dominant by couple of orders of magnitude. This enhanced donor-donor energy transfer can be attributed to high donor concentration, for which the donor to acceptor energy transfer takes place through donor–donor energy migration mechanism. As observed in present situation of $C_{DD} > C_{DA}$, it is suggested that migration occurs by hopping mechanism; thus Burshtein model is expected to fit with respective decay curve.

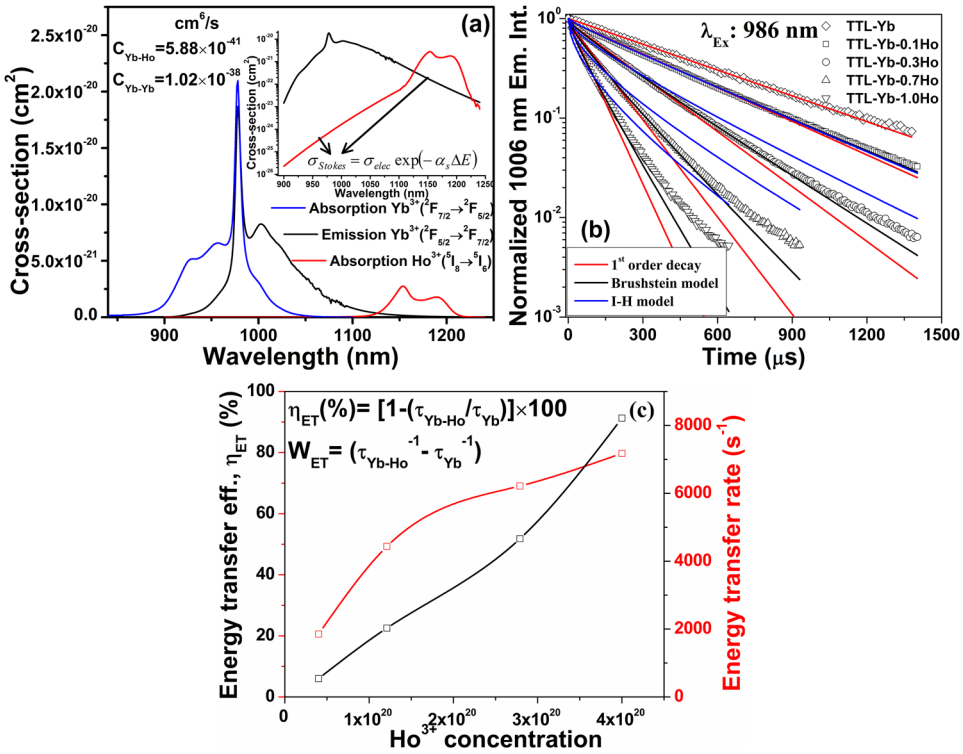

FIG. 6. (a) Absorption and emission cross-section for Yb^{3+} ion with absorption cross-section Ho^{3+}: $^5I_8 \rightarrow {}^5I_6$ transition to estimate the energy transfer micro-parameters via Förster-Dexter method (inset: Stokes extended cross-section for absorption and emission bands), (b) semi-log plot of time dependent normalized 1010nm emission intensity for Yb^{3+} and Ho^{3+}/Yb^{3+} codoped glasses fitted with single exponential function, Brushstein and Inokuti-Hirayama equations, (c) Ho^{3+} ion concentration dependent energy transfer efficiency (η_{ET}) and energy transfer rate (W_{ET}).

TABLE V. Experimental determination of the regression coefficient (R^2) of fitting, energy transfer micro-parameter (C_{DA}, cm^6/s), energy transfer rate (γ^2, s^{-1}) and migration rate (W_m, s^{-1}) for Brushstein and Inokuti-Hirayama model.

	Brushstein				Inokuti-Hirayama		
Sample	R^2	C_{DA} ($\times 10^{-40}$)	γ^2	W_m	R^2	C_{DA} ($\times 10^{-40}$)	γ^2
TTL-Yb-0.1Ho	0.99958	7.74	68	40	0.99954	6.25	55
TTL-Yb-0.3Ho	0.99923	4.50	358	1050	0.99245	15.8	1257
TTL-Yb-0.7Ho	0.99762	2.89	1249	2980	0.97849	12.4	5366
TTL-Yb-1.0Ho	0.99515	2.19	1931	6420	0.96345	13.7	12044
Förster-Dexter	C_{DA} (cm^6/s)				C_{DD} (cm^6/s)		
	5.88×10^{-41}				1.02×10^{-38}		

E. Decay kinetics and fluorescence lifetime

Standard energy transfer models like Brushtein, Inokuti-Hirayama (I-H) models were adopted to predict the probable mechanisms and respective fitting curves are presented in Fig. 6(b).[37] The Inokuti-Hirayama model can be expressed as:

$$I(t) = I_0 \exp\left[-(t/\tau_0) - \left\{(4\pi/3)N_A\Gamma(1-3/s)(C_{DA}t)^{3/s}\right\}\right] \quad (10)$$

where N_A is the acceptor ion concentration; Γ is the Euler's gamma function; s is the electrostatic interaction parameter (for dipole-dipole interaction s = 6); C_{DA} is the microscopic energy transfer parameter between donor-acceptor; the intrinsic lifetime of donor ion is (τ_0), can be evaluated as lifetime of donor ion at smallest possible concentration. The lifetime of 1006nm of 0.1mol% Yb_2O_3 doped TTL glass has been evaluated as 434μs, which has been considered as τ_0 for present situation. This I-H model is applicable for the direct donor-to-acceptor energy transfer processes. However, as reported by Sontakke *et. al.*, donor-donor migration assisted energy transfer is a possible alternative mechanism which can be realized on the basis of Brushtein model.[37] Brushtein model can be presented as:

$$I(t) = I_0 \exp\left[-(t/\tau_0) - \left\{(4\pi/3)N_A\Gamma(1-3/s)(C_{DA}t)^{3/s}\right\} - W_m t\right] \quad (11)$$

In the above equation (W_m, s^{-1}) is the migration parameter while all other terms has same meaning as mentioned above. The fitting parameters like regression coefficient (R^2), energy transfer rate (γ^2, s^{-1}), donor-acceptor micro-parameter (C_{DA}, cm^6s^{-1}), and energy migration rate (W_m, s^{-1}) have been presented in Table V. The regression coefficient represents the goodness of fit of the respective models, regarding the Ho^{3+}/Yb^{3+} codoped TTL glasses; regression coefficient is higher for Brushtein over I-H model. Unlike the donor-acceptor (i.e. direct energy transfer), Brushstein model signifies the donor-donor migration assisted energy transfer (i.e. indirect energy transfer).[42,43] Table V suggests that Brushtein model is fitting precisely compare to I-H model and this has been in accordance with the Förster-Dexter model of spectral overlap. Using the lifetime for Yb^{3+} singly doped and mean lifetime of Yb^{3+} emission for Ho^{3+}/Yb^{3+} codoped glasses the energy transfer efficiency (η_{ET}) has been estimated and presented in Fig. 6(c). According to the Fig. 6(b), the I-H and Brushstein models are fitted precisely for TTL-Yb-0.1Ho sample. Since, for 0.1 mol% concentration of Ho_2O_3, the probability of donor-donor interaction is significantly low, therefore direct donor-acceptor energy transfer (i.e. I-H) model is more suitable for TTL-Yb-0.1Ho sample. However, with the increase of Ho^{3+} concentration in the co-doped glass, the Brushstein model is fitting precisely; whereas, I-H model has been progressively deviated from the experimental decay curve. Moreover, the probability of donor-donor energy migration has been increased, with the Ho^{3+} concentration in the network. In this regard, the progressive inclusion of Ho^{3+} ion the network has gradually reduced the donor-donor separation, which is effectively enhanced the donor-donor energy migration probability. Consequently, the donor-donor migration assisted energy transfer (i.e. Brushstein) model has been fitted more precisely for the higher concentration (≥ 0.3 mol %) of Ho^{3+} ion in co-doped glass. In case of Ho^{3+}/Yb^{3+} codoped system, energy transfer efficiency (η_{ET}) increases with the Ho^{3+} concentration; however, Fig. 4(a) implies that Ho^{3+}:$^5I_6$ level related maximum luminescence intensity has been achieved from TTL-Yb-0.7Ho glass. The possible reason for this could be, an efficient energy transfer Yb^{3+}:$^2F_{5/2}$→Ho^{3+}:$^5I_6$ followed by concentration quenching in Ho^{3+}:$^5I_6$ level. For the present series of Ho^{3+} singly doped glasses, the fluorescence lifetime corresponding to Ho: $^5I_6$ level is 80– 85μs, under 0.896μm excitation. On the other hand, for the Ho^{3+}/Yb^{3+} codoped glasses under Yb^{3+} sensitization, single exponential experimental lifetime has been evaluated as 466, 280, 176 and 125μs for TTL-Yb-0.1Ho, TTL-Yb-0.3Ho, TTL-Yb-0.7Ho and TTL-Yb-1.0Ho respectively. The enhancement in fluorescence lifetime for Ho: $^5I_6$ manifold under Yb^{3+} sensitization can be attributed to the efficient Yb^{3+}→Ho^{3+} energy transfer. The enhancement in fluorescence lifetime for Ho: $^5I_6$ level under Yb^{3+} sensitization is responsible for the improvement in emission intensity associated to Ho: $^5I_6$ level in Ho^{3+}/Yb^{3+}-codoped TTL glasses. Therefore, significant enhancement in luminescence intensity has been achieved, for NIR (2.05μm) and MIR (2.88μm) band in Ho^{3+}/Yb^{3+}-codoped TTL glasses.

IV. CONCLUSIONS

In summary, a series of low phonon (~750 cm^{-1}) TeO_2–TiO_2–La_2O_3 (TTL) glasses were fabricated by melt-quenching technique with Ho^{3+} doping as well as Ho^{3+}/Yb^{3+} codoping. Judd-Ofelt analysis reveals that radiative transition probabilities related to possible MIR (2.88μm) and NIR (2.05μm) emission, corresponding to

radiative transition probabilities, are 34.4 and 132.4s^{-1} respectively; and they appear to be higher than those of ZBLAN and oxyfluoride glasses. The low phonon energy of the present host is responsible for experimental realization of probable inter-manifold emission transitions like $^5(S_2, F_4)\rightarrow{}^5I_{7,6,5}$; $^5F_5\rightarrow{}^5I_7$ and $^5I_6\rightarrow{}^5I_7$ from Ho^{3+}: TTL glasses extended from visible to MIR range. However intense NIR and MIR emission bands were achieved from Ho^{3+}/Yb^{3+} codoped TTL glasses under Yb^{3+} sensitization. Broadband (FWHM, $\Delta\lambda$= 180nm) MIR emission with peak wavelength at 2.88μm has been realized from Ho^{3+}: $^5I_6\rightarrow{}^5I_7$ transition with stimulated emission cross section $4.5\times10^{-21}cm^2$; accordingly the gain bandwidth was estimated to be $7.67\times10^{-26}cm^3$. Apart from MIR, broad (FWHM, $\Delta\lambda$= 160.5nm) NIR emission peak at 2.04μm has been realized from present host. The gain cross-section for present host suggests that lower threshold lasers can be accomplished from present host. The Förster-Dexter theory for non-resonant energy transfer was applied to quantify the energy transfer microparameters C_{DD} and C_{DA} as 1.02×10^{-38} and $5.88\times10^{-41}cm^6/s$ respectively, implying that the migration assisted energy transfer. Further, the low melting temperature (900^0C), cost effective and uncomplicated synthesis technique with phonon energy amounting to ~750cm^{-1}, 50% transmission cutoff wavelength (5.5μm) and material zero dispersion wavelengths (2.28μm) were projecting the effectiveness of TeO_2–TiO_2–La_2O_3 glass as a potential solid state broadband laser material. The collective consequences suggest that Ho^{3+}/Yb^{3+}-codoped TeO_2–TiO_2–La_2O_3 glasses are promising oxide glasses and can be superior candidates for compact and solid-state MIR as well as NIR laser materials.

ACKNOWLEDGMENTS

Authors would like to thank Dr. K. Muraleedharan, Director, CSIR-CGCRI and Dr Ranjan Sen, Head, Glass Division for their kind encouragement and permission to publish this work. One of the authors (GG) is thankful to BRNS/DAE for financial support in the form of Senior Research Fellowship.

REFERENCES

[1] W. B. Grant, R. H. Kagann, and W. A. McClenny, J. Air Waste Manag. Assoc. **42**, 18 (1992).
[2] T. Schweizer, B. N. Samson, J. R. Hector, W. S. Brocklesby, D. W. Hewak, and D. N. Payne, Infrared Phys. Technol. **40**, 329 (1999).
[3] A. Godard, C. R. Phys. **8**, 1100 (2007).
[4] S. D. Jackson, Nat. Photonics. **6**, 423 (2012).
[5] Y. Tian, L. Y. Zhang, R. R. Xu, L. L. Hu, and J. J. Zhang, Appl. Phys. B **101**, 861 (2010).
[6] O. A. Louchev, Y. Urata, M. Yumoto, N. Saito, and S. Wada, J. Appl. Phys. **104**, 33114 (2008).
[7] P. Zhang, Y. Hang, and L. Zhang, Opt. Lett. **37**, 5241 (2012).
[8] S. Li, P. Wang, H. Xia, J. Peng, L. Tang, Y. Zhang, and H. Jiang, Chin. Opt. Lett. **12**, 21601 (2014).
[9] G. Chai, G. Dong, J. Qiu, Q. Zhang, and Z. Yang, J. Phys. Chem. C **116**, 19941 (2012).
[10] X. Wu and K. W. Kwok, J. Am. Ceram. Soc. **97**, 1504 (2014).
[11] S. Chenu, E. Véron, C. Genevois, G. Matzen, T. Cardinal, A. Etienne, D. Massiot, and M. Allix, Adv. Opt. Mater. **2**, 364 (2014).
[12] S. F. Wang, J. Zhang, D. W. Luo, F. Gu, D. Y. Tang, Z. L. Dong, G. E. B. Tan, W. X. Que, T. S. Zhang, S. Li *et al.*, Prog. Solid State Chem. **41**, 20 (2013).
[13] A. Jha, B. D. O. Richards, G. Jose, T. Toney Fernandez, C. J. Hill, J. Lousteau, and P. Joshi, Int. Mater. Rev. **57**, 357 (2012).
[14] G. Gupta, S. Balaji, K. Biswas, and A. Kalyandurg, J. Am. Ceram. Soc. **101**, 3900 (2018).
[15] Y. Tian, R. Xu, L. Hu, and J. Zhang, J. Quant. Spectrosc. Radiat. Transf. **113**, 87 (2012).
[16] L. Wetenkamp, Electron. Lett. **26**, 883 (1990).
[17] K. Biswas, S. Balaji, D. Ghosh, A. D. Sontakke, and K. Annapurna, J. Alloys Compd. **608**, 266 (2014).
[18] K. Yoshimoto, Y. Ezura, M. Ueda, A. Masuno, and H. Inoue, Adv. Opt. Mater. **6**, 1701283 (2018).
[19] B. R. Judd, Phys. Rev. **127**, 750 (1962).
[20] G. S. Ofelt, The J. Chem. Phys. **37**, 511 (1962).
[21] A. D. Sontakke and K. Annapurna, Mater. Chem. Phys. **137**, 916 (2013).
[22] A. A. Kaminskii, *Laser Crystals: Their Physics and Properties* (Springer, 2013).
[23] G. A. Kumar, E. la Rosa-Cruz, K. Ueda, A. Martínez, and O. Barbosa-Garcia, Opt. Mater. **22**, 201 (2003).
[24] H. Ebendorff-Heidepriem, D. Ehrt, M. Bettinelli, and A. Speghini, J. Non-Cryst. Solids **240**, 66 (1998).
[25] E. Oomen and A.-M. A. Van Dongen, J. Non-Cryst. Solids **111**, 205 (1989).
[26] L. Wetenkamp, G. F. West, and H. Többen, J. Non-Cryst. Solids **140**, 35 (1992).
[27] L. Feng, J. Wang, Q. Tang, L. Liang, H. Liang, and Q. Su, J. Lumin. **124**, 187 (2007).
[28] S. Mahamuda, K. Swapna, P. Packiyaraj, A. S. Rao, and G. V. Prakash, Opt. Mater. **36**, 362 (2013).
[29] P. Nachimuthu and R. Jagannathan, J. Am. Ceram. Soc. **82**, 387 (1999).
[30] C. K. Jørgensen and R. Reisfeld, Journal of the Less Common Metals **93**, 107 (1983).
[31] S. Tanabe, T. Hanada, T. Ohyagi, and N. Soga, Phys. Rev. B **48**, 10591 (1993).
[32] Y. Tian, X. Jing, and S. Xu, Spectrochim. Acta A **115**, 33 (2013).
[33] B. Zhou, T. Wei, M. Cai, Y. Tian, J. Zhou, D. Deng, S. Xu, and J. Zhang, J. Quant. Spectrosc. Radiat. Transf. **149**, 41 (2014).
[34] S. Balaji, G. Gupta, K. Biswas, D. Ghosh, and K. Annapurna, Sci. Rep. **6**, 29203 (2016).
[35] S. Wei, Y. Xu, S. Dai, Y. Zhou, C. Lin, and P. Zhang, J. Phys.: Condens. Matter **416**, 64 (2013).
[36] J. Zhang, Y. Lu, M. Cai, Y. Tian, F. Huang, and S. Xu, IEEE Photonics Technol. Lett. **29**, 1498 (2017).
[37] A. D. Sontakke, K. Biswas, R. Sen, and K. Annapurna, J. Opt. Soc. Am. B **27**, 2750 (2010).
[38] J. A. Caird, A. J. Ramponi, and P. R. Staver, J. Opt. Soc. Am. B **8**, 1391 (1991).
[39] R. M. Martin and R. S. Quimby, J. Opt. Soc. Am. B **23**, 1770 (2006).
[40] F. Auzel, Phy. Rev. B **13**, 2809 (1976).
[41] M. C. Nostrand, R. H. Page, and S. A. Payne, J. Opt. Soc. Am. B **18**, 264 (2001).
[42] S. Balaji, A. D. Sontakke, and K. Annapurna, J. Opt. Soc. Am. B **29**, 1569 (2012).
[43] S. Balaji, K. Biswas, A. D. Sontakke, G. Gupta, and K. Annapurna, Spectrosc. Radiat. Transf. **147**, 112 (2014).